Boundary Value Problems
a SpringerOpen Journal

RESEARCH   **Open Access**

The high-order smooth interpolated reproducing kernel particle method for elastodynamics problems

Jinpeng Gu[1], Yixiao Qin[1*] and Zhonghua Li[2]

*Correspondence:
1983015@tyust.edu.cn
[1]College of Mechanical Engineering,
Taiyuan University of Science and
Technology, Taiyuan 030024, China
Full list of author information is
available at the end of the article

Abstract

Combining the interpolation reproducing kernel particle method (IRKPM) with the integral weak form of elastodynamics, we present a high-order smooth interpolated reproducing kernel particle method for an elastodynamics plane problem. The shape function of IRKPM not only has the interpolation property at any point but also has a high-order smoothness not lower than that of the kernel function. This new method overcomes the difficulties of most meshless methods in dealing with essential boundary conditions and ensures high numerical accuracy. For time domain integration, we use the classical Newmark average acceleration method. By numerical examples we demonstrate that the proposed method has the advantages of higher accuracy, smaller scale of solving problem, and direct application of boundary conditions.

Keywords: Meshless method; Interpolated reproducing kernel particle method; Elastodynamics; High-order smooth algorithm

1 Introduction

The beams, plates and shells, widely used in engineering, are often affected by vibration and impact. The finite element method depends on the mesh division to deal with such problems [1, 2]. When the mesh is distorted, the accuracy of the results obtained by the finite element method decreases. The meshless method adopts point-based approximation and can ignore the influence of mesh distortion when dealing with numerical problems [3]. The meshless method has the advantages of saving analysis time and ensuring calculation accuracy, which at present is the hot spot and development direction of scientific and engineering calculation methods [4].

In the calculation process, only node information is needed, which overcomes the limitation of connecting nodes to elements between nodes [5]. The meshless method can easily deal with the problems of large deformation [6], crack-growth processes [7], convection heat transfer [8], fluid-structure interaction [9], and elastodynamics [10, 11].

With the rapid development of computer technology and calculation method, various numerical methods have become important means to solve scientific and engineering problems [12–17]. As an important scientific problem, structural dynamic analysis has

been paid more attention in various fields [18–21]. In this case, the finite element method (FEM), as the most general numerical method, becomes the main method for dynamic analysis and nonlinear analysis [22, 23]. The FEM for solving structural dynamic problems depends on the division and refinement of elements [24]. In the case of complex geometry, stress singularities and concentration occur unless a high-quality finite element mesh is generated at a very time consuming and tedious cost [25]. The output result of the quadratic approximation will be distorted when the discontinuity stress related to the elements is in the area of the stress concentration [26]. The meshless methods were first used to simulate celestial phenomena without boundaries [27, 28]. The meshless method uses the approximation of the point, and the displacement trial function of the calculation point is only associated with the shape function of the discrete point in the influence domain. Without the dependence of the grids, the output displacement, strain, and stress are continuous in the whole analysis domain, and the error of the quadratic approximation is avoided [29, 30]. Two mainstream meshless methods are the element-free Galerkin methods [31–35] and the reproducing kernel particle methods [36–39]. However, the meshless method based on the Galerkin discretization scheme is not easy to apply the boundary conditions.

Dynamic analysis is an important step in the evaluation of elastic structures. Meshless methods take particles as basic computing units, and there is no need to establish fixed topological relations between particles, so they are suitable for solving elastic dynamic problems [40, 41]. Several authors have attempted to apply meshless methods to elastodynamics problems. Selecting an appropriate form function can reduce the computational cost [42]. A meshless local integral method for two-dimensional elastodynamic fracture problems by the Laplace transform technique is proposed [43]. The Newmark method is generally selected as an approximation scheme to deal with time-dependent cases [44–46].

In this paper, combining the IRKPM with the integral weak form governing equation of elastodynamics, we establish a high-order smooth interpolated reproducing kernel particle method for two-dimensional elastodynamics problems. We derive the corresponding discrete equations and adopt the time domain integration the Newmark constant average acceleration method. This method adopts point-based approximation, which can ignore the influence of grid distortion in the dynamic analysis, save the analysis time, and ensure the calculation accuracy. This method can easily apply boundary conditions like the finite element method and can avoid the difficulties in dealing with the boundary condition. Compared with other meshless methods, this method has the character of directly applying boundary conditions, a small amount of calculation, and high accuracy. The correctness and effectiveness of this method are proved by some numerical examples.

2 The basic equation of elastic mechanics

Let Ω be the domain of problem with boundary Γ. For linear elastic problem, $\boldsymbol{b}$ is the body force, $\bar{\boldsymbol{t}}$ is the known surface force on the natural boundary, $\bar{\boldsymbol{u}}$ is the known displacement on essential boundary, and $\boldsymbol{n}$ is the directional cosine matrix at the point $\boldsymbol{x}$ on the natural boundary. The basic equations of two-dimensional elastic mechanics are

$$\boldsymbol{L}^{\mathrm{T}}\boldsymbol{\sigma} + \boldsymbol{b} - \rho\ddot{\boldsymbol{u}} - \mu\dot{\boldsymbol{u}} = \boldsymbol{0} \quad \text{in } \Omega, \tag{1}$$

$$\boldsymbol{\varepsilon} = \boldsymbol{L}\boldsymbol{u} \quad \text{in } \Omega, \tag{2}$$

$$\sigma = D\varepsilon \quad \text{in } \Omega, \tag{3}$$

$$\sigma n = \bar{t} \quad \text{on } \Gamma_u, \tag{4}$$

$$u = \bar{u} \quad \text{on } \Gamma_t, \tag{5}$$

$$u(x, t_0) = u_0(x), \quad x \in \Omega, \tag{6}$$

$$\dot{u}(x, t_0) = v_0(x), \quad x \in \Omega, \tag{7}$$

where L is the differential operator matrix

$$L = \begin{bmatrix} \frac{\partial}{\partial x_1} & 0 & \frac{\partial}{\partial x_2} \\ 0 & \frac{\partial}{\partial x_2} & \frac{\partial}{\partial x_1} \end{bmatrix}^{\mathrm{T}}, \tag{8}$$

ρ is the density, μ is the damping coefficient, $-\mu\dot{u}$ is the damping force, $-\rho\ddot{u}$ is the inertia force;

$$\sigma = \begin{bmatrix} \sigma_{11}(t) & \sigma_{22}(t) & \sigma_{12}(t) \end{bmatrix}^{\mathrm{T}}, \tag{9}$$

$$b = \begin{bmatrix} b_1(t) & b_2(t) \end{bmatrix}^{\mathrm{T}}, \tag{10}$$

$$\varepsilon = \begin{bmatrix} \varepsilon_{11}(t) & \varepsilon_{22}(t) & \varepsilon_{12}(t) \end{bmatrix}^{\mathrm{T}}, \tag{11}$$

$$u = \begin{bmatrix} u(t) & v(t) \end{bmatrix}^{\mathrm{T}}, \tag{12}$$

where σ, b, ε, and u are the stress vector, body force vector, strain matrix, and displacement matrix at any point on the domain, respectively;

$$\dot{u}^{\mathrm{T}} = (\dot{u}(t), \dot{v}(t)), \tag{13}$$

$$\ddot{u}^{\mathrm{T}} = (\ddot{u}(t), \ddot{v}(t)), \tag{14}$$

where $\dot{u}$ and $\ddot{u}$ are the first and second derivatives of the displacement matrix u, respectively.

Let D be the elasticity matrix. The plane stress matrix can be expressed as

$$D = \frac{E}{1 - \mu^2} \begin{bmatrix} 1 & \mu & 0 \\ \mu & 1 & 0 \\ 0 & 0 & \frac{1-\mu}{2} \end{bmatrix}, \tag{15}$$

where E is Young's modulus, and μ is Poisson's ratio.

3 Interpolated reproducing kernel particle method for elastodynamics problems

3.1 Shape function of the interpolated reproducing kernel particle method

When the number of nodes in the compact support domain is greater than the number of the basis function monomials, we construct the interpolating shape function of the improved reproducing kernel particle method.

The cubic spline function is adopted as a weight function, that ism

$$\hat{\Phi}_{\hat{a}_I}(\pmb{x} - \pmb{x}_I) = \Phi(d) = \begin{cases} \frac{2}{3} - 4d^2 + 4d^3, & d \leq \frac{1}{2}, \\ \frac{4}{3} - 4d + 4d^2 - \frac{4}{3}d^3, & \frac{1}{2} < d \leq 1, \\ 0, & d > 1. \end{cases} \tag{16}$$

Let the improved interpolating nuclear particle of $u(x)$ be approximately

$$u^a(\pmb{x}) = \sum_{I=1}^{NP} \Psi_I(\pmb{x}) u_I, \tag{17}$$

where the shape function of the improved interpolating kernel particle is

$$\Psi_I(\pmb{x}) = \hat{\Psi}_I(\pmb{x}) + \bar{\Psi}_I(\pmb{x}), \tag{18}$$

with a function $\hat{\Psi}_I(\pmb{x})$ that possesses the Kronecker delta property and an enhanced function $\bar{\Psi}_I(\pmb{x})$ in the form of IRKPM. Therefore the constructed shape function has the property of interpolating on any point and a higher-order smoothness not less than that of the kernel function.

The improved second-order interpolating condition of the interpolating kernel particle shape function $\Psi_I(\pmb{x})$ can be given as

$$\sum_{I=1}^{NP} \big[\hat{\Psi}_I(\pmb{x}) + \bar{\Psi}_I(\pmb{x})\big] x_I^\alpha = x^\alpha, \quad |\alpha| \leq 2. \tag{19}$$

If the simple function $\hat{\Psi}_I(\pmb{x})$ satisfies the Kronecker delta property, that is, $\hat{\Psi}_I(\pmb{x}_J) = \delta_{IJ}$, and Eq. (19) holds, then the enhancement function vector is as follows:

$$\bar{\pmb{\Psi}}(\pmb{x}) = \big\{\bar{\Psi}_1(\pmb{x}), \bar{\Psi}_2(\pmb{x}), \ldots, \bar{\Psi}_{NP}(\pmb{x})\big\}. \tag{20}$$

The basis vectors made up of moving monomials, which are orthogonal, can be written as

$$\pmb{h}_i(\pmb{x}) = \big\{h_i(\pmb{x} - \pmb{x}_1), h_i(\pmb{x} - \pmb{x}_2), \ldots, h_i(\pmb{x} - \pmb{x}_{NP})\big\}, \tag{21}$$

$$\pmb{H}(\pmb{x} - \pmb{x}_I) = \big[1, x_1 - x_{I1}, \ldots, x_d - x_{Id}, (x_1 - x_{I1})^2, \ldots, (x_d - x_{Id})^n\big]^{\mathrm{T}}, \tag{22}$$

where the ith element of $\pmb{H}(\pmb{x} - \pmb{x}_I)$, for example, for all discrete points $\{\pmb{x}_J\}_{J=1}^{NP}$, is

$$\bar{\pmb{\Psi}}(\pmb{x}_J)^{\mathrm{T}} \pmb{h}_i(\pmb{x}_J) = 0 \quad \forall J. \tag{23}$$

In view of Eq. (19), Eq. (23) can be rewritten as

$$\sum_{I=1}^{NP} \big[\hat{\Psi}_I(\pmb{x}) + \bar{\Psi}_I(\pmb{x})\big] \pmb{H}(\pmb{x} - \pmb{x}_I) = \pmb{H}(\pmb{0}). \tag{24}$$

For $\boldsymbol{x}_J$, we have

$$\sum_{I=1}^{NP}\left[\hat{\Psi}_I(\boldsymbol{x}_J) + \bar{\Psi}_I(\boldsymbol{x}_J)\right]\boldsymbol{H}(\boldsymbol{x}_J - \boldsymbol{x}_I) = \boldsymbol{H}(\boldsymbol{0}). \tag{25}$$

If $\hat{\Psi}_I(\boldsymbol{x}_J) = \delta_{IJ}$ and any J point satisfies $\sum_{I=1}^{NP}\delta_{IJ}\boldsymbol{H}(\boldsymbol{x}_J - \boldsymbol{x}_I) = \boldsymbol{H}(\boldsymbol{0})$, then based on the last equation, we have

$$\sum_{I=1}^{NP}\bar{\Psi}_I(\boldsymbol{x}_J)\boldsymbol{H}(\boldsymbol{x}_J - \boldsymbol{x}_I) = \boldsymbol{0}. \tag{26}$$

We can obtain the equivalent equation

$$\sum_{I=1}^{NP}\bar{\Psi}_I(\boldsymbol{x}_J)h_i(\boldsymbol{x}_J - \boldsymbol{x}_I) = 0. \tag{27}$$

Thus we obtained Eq. (23).

Let

$$\bar{\Psi}_I(\boldsymbol{x}) = \boldsymbol{G}^{\mathrm{T}}(\boldsymbol{x} - \boldsymbol{x}_I)\boldsymbol{b}(\boldsymbol{x}), \tag{28}$$

where $\boldsymbol{G}(\boldsymbol{x} - \boldsymbol{x}_I)$ is the vector of basis functions that has the same dimension as $\boldsymbol{H}(\boldsymbol{x}_J - \boldsymbol{x}_I)$, and $\boldsymbol{b}(\boldsymbol{x})$ is the corresponding coefficient vector. Substituting Eq. (28) into Eq. (26) we have

$$\boldsymbol{Q}(\boldsymbol{x}_J)\boldsymbol{b}(\boldsymbol{x}_J) = \boldsymbol{0}, \tag{29}$$

where

$$\boldsymbol{Q}(\boldsymbol{x}) = \sum_I \boldsymbol{H}(\boldsymbol{x} - \boldsymbol{x}_I)\boldsymbol{G}^{\mathrm{T}}(\boldsymbol{x} - \boldsymbol{x}_I). \tag{30}$$

If $\boldsymbol{Q}(\boldsymbol{x}_J)$ is nonsingular, then from Eq. (29) we obtain $\boldsymbol{b}(\boldsymbol{x}_J) = \boldsymbol{0}$. Since $\bar{\Psi}_I(\boldsymbol{x}_J) = 0$ by Eq. (28), we get

$$\Psi_I(\boldsymbol{x}_J) = \bar{\Psi}_I(\boldsymbol{x}_J) + \widehat{\Psi}_I(\boldsymbol{x}_J) = \delta_{IJ}. \tag{31}$$

To make $\boldsymbol{Q}(\boldsymbol{x})$ nonsingular, an obvious choice for $\boldsymbol{G}(\boldsymbol{x} - \boldsymbol{x}_I)$ is

$$\boldsymbol{G}(\boldsymbol{x} - \boldsymbol{x}_I) = \boldsymbol{H}(\boldsymbol{x} - \boldsymbol{x}_I)\bar{\Phi}_{\bar{a}_I}(\boldsymbol{x} - \boldsymbol{x}_I), \tag{32}$$

where $\bar{\Phi}_{\bar{a}_I}(\boldsymbol{x} - \boldsymbol{x}_I) \geq 0$ is a weight function with compact support. So

$$\bar{\Psi}_I(\boldsymbol{x}) = \boldsymbol{H}^{\mathrm{T}}(\boldsymbol{x} - \boldsymbol{x}_I)\boldsymbol{b}(\boldsymbol{x})\bar{\Phi}_{\bar{a}_I}(\boldsymbol{x} - \boldsymbol{x}_I). \tag{33}$$

As we can see from the above, if the enhancement function is of the form (28) and the simple function has the Kronecker delta property, then the interpolation function $\Psi_I(\boldsymbol{x})$ will be generated if Eq. (19) is satisfied.

The coefficient $\boldsymbol{b}(\boldsymbol{x})$ of $\bar{\Psi}_I(\boldsymbol{x})$ can be obtained by the condition of reproducing, and $\hat{\Psi}_I(\boldsymbol{x})$ can be expressed as

$$\hat{\Psi}_I(\boldsymbol{x}) = \frac{\hat{\Phi}_{\hat{a}_I}(\boldsymbol{x} - \boldsymbol{x}_I)}{\hat{\Phi}_{\hat{a}_I}(\boldsymbol{0})}, \quad \hat{a}_I < \min\{\|\boldsymbol{x}_I - \boldsymbol{x}_J\| \ \forall J \neq I\}, \tag{34}$$

where $\hat{\Psi}_I(\boldsymbol{x})$ satisfies the Kronecker delta condition.

Substituting Eqs. (33) and (34) into Eq. (18) yields

$$\sum_{I=1}^{NP}\left[\hat{\Psi}_I(\boldsymbol{x}) + \boldsymbol{H}^{\mathrm{T}}(\boldsymbol{x} - \boldsymbol{x}_I)\boldsymbol{b}(\boldsymbol{x})\hat{\Phi}_{\hat{a}_I}(\boldsymbol{x} - \boldsymbol{x}_I)\right]\boldsymbol{x}_I^\alpha = \boldsymbol{x}^\alpha, \quad |\alpha| \leq n. \tag{35}$$

From Eq. (35) we have

$$\sum_{I=1}^{NP}\boldsymbol{H}(\boldsymbol{x} - \boldsymbol{x}_I)\left[\hat{\Psi}_I(\boldsymbol{x}) + \boldsymbol{H}^{\mathrm{T}}(\boldsymbol{x} - \boldsymbol{x}_I)\boldsymbol{b}(\boldsymbol{x})\hat{\Phi}_{\hat{a}_I}(\boldsymbol{x} - \boldsymbol{x}_I)\right] = \boldsymbol{H}(\boldsymbol{0}). \tag{36}$$

The coefficient vector $\boldsymbol{b}(\boldsymbol{x})$ can be obtained as

$$\boldsymbol{b}(\boldsymbol{x}) = \boldsymbol{Q}^{-1}(\boldsymbol{x})\left[\boldsymbol{H}(\boldsymbol{0}) - \hat{\boldsymbol{H}}(\boldsymbol{x})\right], \tag{37}$$

where

$$\hat{\boldsymbol{H}}(\boldsymbol{x}) = \sum_{I=1}^{NP}\boldsymbol{H}(\boldsymbol{x} - \boldsymbol{x}_I)\hat{\Psi}_I(\boldsymbol{x}). \tag{38}$$

Finally, we obtain the interpolation shape function of the improved reproducing kernel particle as follows:

$$\Psi_I(\boldsymbol{x}) = \hat{\Psi}_I(\boldsymbol{x}) + \boldsymbol{H}^{\mathrm{T}}(\boldsymbol{x} - \boldsymbol{x}_I)Q^{-1}(x)\left[\boldsymbol{H}(\boldsymbol{0}) - \hat{\boldsymbol{H}}(\boldsymbol{x})\right]\bar{\Phi}_{\bar{a}_I}(\boldsymbol{x} - \boldsymbol{x}_I). \tag{39}$$

As Fig. 1 shows, 121 particles are nonuniformly put on the 2D domain $(x, y) \in [0, 10] \times [0, 10]$, the cubic spline functions are taken as the weight functions of $\hat{\Phi}_{\hat{a}_I}(\boldsymbol{x} - \boldsymbol{x}_I)$ and $\bar{\Phi}_{\bar{a}_I}(\boldsymbol{x} - \boldsymbol{x}_I)$, $\hat{a}_1 = 0.48d_c$, $\bar{a} = 3.0d_c$, and $\hat{\Psi}_I(\boldsymbol{x})$ is the minimum particle spacing. Then the shape functions of the asterisk particle are shown in Fig. 1.

Figure 1 illustrates that the shape function has an excellent characteristic of node interpolation. The displacement, stress, and strain obtained by this method have smooth continuity on the whole domain and avoid the calculation error from the finite element method.

We analyze the reproducing kernel shape function and its interpolation properties in particular cases and study the construction process of the interpolation shape function of the improved reproducing kernel particle. We can see from these figures that the improved reproducing kernel shape function has good interpolation characteristics. Theoretically, the smoothness of the shape function of the improved reproducing kernel particle is guaranteed to be no less than that of the weight function.

The interpolation form function of the improved reproducing kernel particle is based on the coupling of a simple function with the Kronecker delta property and an enhanced

Figure 1 Shape functions of 2D IRKPM with nonuniform particles
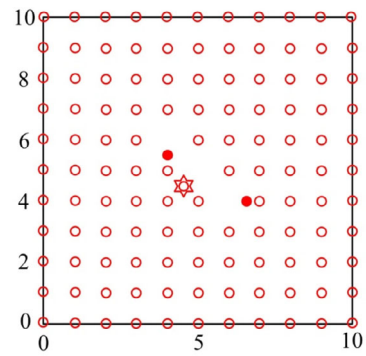
(a) Particle arrangement

(b) $\hat{\Psi}_I(\boldsymbol{x})$

(c) $\overline{\Psi}_I(\boldsymbol{x})$
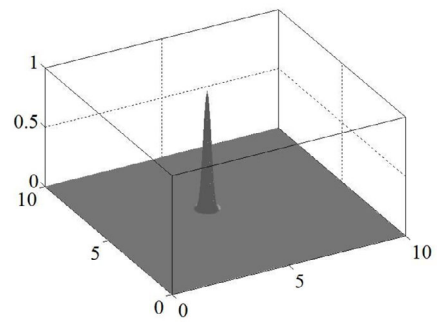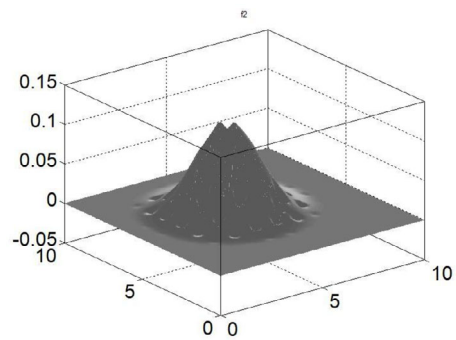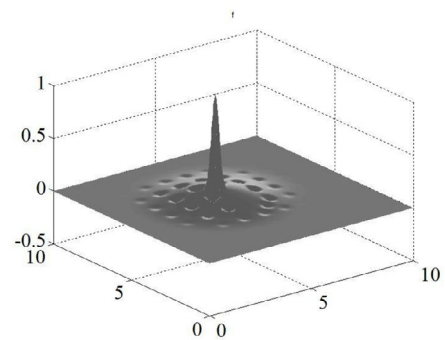
(d) $\Psi_I(\boldsymbol{x})$

function of IRKPM shape function format. When the original simple function is used to introduce the discrete Kronecker delta property and the enhancement function is used to construct the reproducing condition, if the enhancement function vector of the discrete point and the basis function vector of the moving monomial satisfy the orthogonality condition, then the shape function of the improved reproducing kernel particle with the Kronecker delta property is obtained. This makes it convenient to directly apply displacement boundary conditions.

3.2 Numerical equations of elastodynamics problems

In the domain $\boldsymbol{\Omega}$ the displacement $\boldsymbol{u} = [u \ \ v]^{\mathrm{T}}$ of any point $\boldsymbol{x}$ at any time t can be written as

$$\boldsymbol{u} = \boldsymbol{\psi}\boldsymbol{u}^n, \tag{40}$$

where $n = NP \leq m$, m is the total number of discrete notes in elasticity domain Ω, and

$$\boldsymbol{\psi} = \begin{bmatrix} \boldsymbol{\psi}_1 & \boldsymbol{\psi}_2 & \cdots & \boldsymbol{\psi}_n \end{bmatrix}, \tag{41}$$

$$\boldsymbol{u}^n = \begin{bmatrix} \boldsymbol{u}_1^{\mathrm{T}} & \boldsymbol{u}_2^{\mathrm{T}} & \cdots & \boldsymbol{u}_n^{\mathrm{T}} \end{bmatrix}^{\mathrm{T}}, \tag{42}$$

where $\boldsymbol{\psi}$ is the shape function, and $\boldsymbol{u}^n$ is the displacement vector of n discrete points on compact support domain of the point $\boldsymbol{x}$.

Setting $I = 1, 2, \ldots, n$, $\boldsymbol{\Psi}_I$ is the shape function submatrix of any particle $\boldsymbol{x}_I$, $\boldsymbol{u}_I$ is the displacement vector of any particle $\boldsymbol{x}_I$, and we have

$$\boldsymbol{\psi}_I = \begin{bmatrix} \Psi_I & 0 \\ 0 & \Psi_I \end{bmatrix}, \tag{43}$$

$$\boldsymbol{u}_I = \begin{bmatrix} u_I & v_I \end{bmatrix}^{\mathrm{T}}. \tag{44}$$

3.3 High-order smooth elastodynamic algorithm

Based on the meshless shape function of any discrete point with smooth interpolation property, a higher-order smooth displacement function can be constructed as follows.

The speed and acceleration at any time t at any point $\boldsymbol{x}$ on the domain can be written as

$$\dot{\boldsymbol{u}} = \sum_I^n \boldsymbol{\psi}_I \dot{\boldsymbol{u}}_I, \tag{45}$$

$$\ddot{\boldsymbol{u}} = \sum_I^n \boldsymbol{\psi}_I \ddot{\boldsymbol{u}}_I, \tag{46}$$

where $\dot{\boldsymbol{u}}_I$ and $\ddot{\boldsymbol{u}}_I$ are the speed and acceleration of the point $\boldsymbol{x}$ at time t, respectively, and they can be written as

$$\dot{\boldsymbol{u}}_I = \begin{bmatrix} \dot{u}_I & \dot{v}_I \end{bmatrix}^{\mathrm{T}}, \tag{47}$$

$$\ddot{\boldsymbol{u}}_I = \begin{bmatrix} \ddot{u}_I & \ddot{v}_I \end{bmatrix}^{\mathrm{T}}. \tag{48}$$

The strain of a point $\boldsymbol{x}$ can be obtained from Eqs. (2) and (40):

$$\boldsymbol{\varepsilon} = \boldsymbol{L}\boldsymbol{u} = \boldsymbol{B}\boldsymbol{u}^n, \tag{49}$$

$$\boldsymbol{B} = \begin{bmatrix} \boldsymbol{B}_1 & \boldsymbol{B}_2 & \cdots & \boldsymbol{B}_n \end{bmatrix}, \tag{50}$$

where $\boldsymbol{B}$ is the strain matrix, and the submatrix $\boldsymbol{B}_I$ of the strain matrix at a particle $\boldsymbol{x}_I$ is

$$\boldsymbol{B}_I = \begin{bmatrix} \frac{\partial \Psi_I}{\partial x_1} & 0 \\ 0 & \frac{\partial \Psi_I}{\partial x_2} \\ \frac{\partial \Psi_I}{\partial x_2} & \frac{\partial \Psi_I}{\partial x_1} \end{bmatrix}. \tag{51}$$

By the virtual work principle of elastic mechanics we have

$$\delta \Pi = -\int_{\Omega} (\boldsymbol{\sigma} - \rho \ddot{\boldsymbol{u}} - \mu \dot{\boldsymbol{u}} + \boldsymbol{b}) \delta \boldsymbol{u} \, d\Omega + \int_{\Gamma_t} (\boldsymbol{\sigma}\boldsymbol{n} - \bar{\boldsymbol{t}}) \delta \boldsymbol{u} \, d\Gamma = 0, \tag{52}$$

i.e.,

$$\int_{\Omega} (\boldsymbol{D}\varepsilon\delta\varepsilon + \rho\ddot{\boldsymbol{u}}\delta\boldsymbol{u} - \mu\dot{\boldsymbol{u}}\delta\boldsymbol{u}) \, d\Omega - \left(\int_{\Omega} \boldsymbol{b}\delta\boldsymbol{u} \, d\Omega - \int_{\Gamma_t} \bar{\boldsymbol{t}}\delta\boldsymbol{u} \, d\Gamma \right) = 0. \tag{53}$$

By Eqs. (40), (45), (46), and (49) we can obtain the following equation:

$$\begin{aligned}
\int_{\Omega} \delta \left(\sum_I^n \boldsymbol{\psi}_I \boldsymbol{u}_I \right)^{\mathrm{T}} \rho \left(\sum_J^n \boldsymbol{\psi}_J \ddot{\boldsymbol{u}}_J \right) \, d\Omega &+ \int_{\Omega} \delta \left(\sum_I^n \boldsymbol{\psi}_I \boldsymbol{u}_I \right)^{\mathrm{T}} \mu \left(\sum_J^n \boldsymbol{\psi}_J \dot{\boldsymbol{u}}_J \right) \, d\Omega \\
&+ \int_{\Omega} \delta \left(\sum_I^n \boldsymbol{B}_I \boldsymbol{u}_I \right)^{\mathrm{T}} \boldsymbol{D} \left(\sum_J^n \boldsymbol{B}_J \boldsymbol{u}_J \right) \, d\Omega - \int_{\Omega} \delta \left(\sum_I^n \boldsymbol{\psi}_I \boldsymbol{u}_I \right)^{\mathrm{T}} \boldsymbol{b} \, d\Omega \\
&- \int_{\Gamma_t} \delta \left(\sum_I^n \boldsymbol{\psi}_I \boldsymbol{u}_I \right)^{\mathrm{T}} \bar{\boldsymbol{t}} \, d\Gamma = 0.
\end{aligned} \tag{54}$$

Because of the arbitrariness of δu, we can write the discrete system equation

$$\boldsymbol{M}\ddot{\boldsymbol{u}} + \boldsymbol{C}\dot{\boldsymbol{u}} + \boldsymbol{K}\boldsymbol{u} = \boldsymbol{f}. \tag{55}$$

If the damping is ignored, Eq. (55) can be simplified as

$$\boldsymbol{M}\ddot{\boldsymbol{u}} + \boldsymbol{K}\boldsymbol{u} = \boldsymbol{f}. \tag{56}$$

If the right-hand item is zero, then this formula is a free vibration equation of the system. $\boldsymbol{u}$, $\dot{\boldsymbol{u}}$, and $\ddot{\boldsymbol{u}}$ are the displacement, speed, and acceleration vectors of the particle, respectively. $\boldsymbol{M}$, $\boldsymbol{C}$, $\boldsymbol{K}$, and $\boldsymbol{f}$ are the quality, damping, stiffness, and particle load matrices, respectively. They can be written as

$$\boldsymbol{u} = \begin{bmatrix} \boldsymbol{u}_1^{\mathrm{T}} & \boldsymbol{u}_2^{\mathrm{T}} & \cdots & \boldsymbol{u}_m^{\mathrm{T}} \end{bmatrix}^{\mathrm{T}}, \tag{57}$$

$$\dot{\boldsymbol{u}} = \begin{bmatrix} \dot{\boldsymbol{u}}_1^{\mathrm{T}} & \dot{\boldsymbol{u}}_2^{\mathrm{T}} & \cdots & \dot{\boldsymbol{u}}_m^{\mathrm{T}} \end{bmatrix}^{\mathrm{T}}, \tag{58}$$

$$\ddot{\boldsymbol{u}} = \begin{bmatrix} \ddot{\boldsymbol{u}}_1^{\mathrm{T}} & \ddot{\boldsymbol{u}}_2^{\mathrm{T}} & \cdots & \ddot{\boldsymbol{u}}_m^{\mathrm{T}} \end{bmatrix}^{\mathrm{T}}, \tag{59}$$

$$\boldsymbol{M}_{IJ} = \int_{\Omega} \boldsymbol{\psi}_I^{\mathrm{T}} \rho \boldsymbol{\psi}_J^{\mathrm{T}} \, \mathrm{d}\Omega \quad (I, J = 1, \dots, m), \tag{60}$$

$$\boldsymbol{C}_{IJ} = \int_{\Omega} \boldsymbol{\psi}_I^{\mathrm{T}} \mu \boldsymbol{\psi}_J^{\mathrm{T}} \, \mathrm{d}\Omega, \tag{61}$$

$$\boldsymbol{K}_{IJ} = \int_{\Omega} \boldsymbol{B}_I^{\mathrm{T}} \boldsymbol{D} \boldsymbol{B}_J \, \mathrm{d}\Omega, \tag{62}$$

$$\boldsymbol{f}_I = \int_{\Omega} \boldsymbol{\psi}_I^{\mathrm{T}} \boldsymbol{b} \, \mathrm{d}\Omega + \int_{\Gamma_t} \boldsymbol{\psi}_I^{\mathrm{T}} \bar{\boldsymbol{t}} \, \mathrm{d}\Gamma, \tag{63}$$

where $I, J = 1, 2, \dots, m$, and $\boldsymbol{K}_{IJ}$, $\boldsymbol{C}_{IJ}$, and $\boldsymbol{f}_I$ are the elements of $\boldsymbol{K}$, $\boldsymbol{C}$, and $\boldsymbol{f}$.

The shape functions of the interpolated reproducing kernel particle all have the characteristics of the Kronecker delta function in a discrete particle, so that the essential boundary can be directly applied.

3.4 Implicit time integration

The time domain is discretized by n time increments. The Newmark method is adopted for the time discretization of the equations of motion. The relationship between the displacement and speed from time t_n to time t_{n+1} can be written as

$$\boldsymbol{u}_{n+1} = \boldsymbol{u}_n + \Delta t \dot{\boldsymbol{u}}_n + \frac{1}{2}(1 - \beta_2)\Delta t^2 \ddot{\boldsymbol{u}}_n + \frac{1}{2}\beta_2 \Delta t^2 \ddot{\boldsymbol{u}}_{n+1}, \tag{64}$$

$$\dot{\boldsymbol{u}}_{n+1} = \dot{\boldsymbol{u}}_n + (1 - \beta_1)\Delta t \ddot{\boldsymbol{u}}_n + \beta_1 \Delta t \ddot{\boldsymbol{u}}_{n+1}, \tag{65}$$

where β_1 and β_2 affect the stability and accuracy of the calculation result. Different parameter selections correspond to different integration methods:

(i) $\beta_1 = \dfrac{1}{2}, \qquad \beta_2 = \dfrac{1}{3}$ (linear acceleration method);

(ii) $\beta_1 = \dfrac{1}{2}, \qquad \beta_2 = \dfrac{1}{2}$ (average acceleration method);

(iii) $\beta_1 = \dfrac{1}{2}, \qquad \beta_2 = 0$ (uniform acceleration method);

(iv) $\beta_1 = \dfrac{3}{2}, \qquad \beta_2 = \dfrac{8}{5}$ (Galerkin method);

(v) $\beta_1 = \dfrac{3}{2}, \qquad \beta_2 = 4$ (backward difference method).

From Eq. (64) we have

$$\ddot{\boldsymbol{u}}_{n+1} = \frac{2}{\beta_2 \Delta t^2}(\boldsymbol{u}_{n+1} - \boldsymbol{u}_n) - \frac{2}{\beta_2 \Delta t}\dot{\boldsymbol{u}}_n - \left(\frac{1}{\beta_2} - 1\right)\ddot{\boldsymbol{u}}_n. \tag{66}$$

Let

$$\alpha_1 = \frac{2}{\beta_2 \Delta t^2}, \tag{67}$$

$$\alpha_2 = \frac{2}{\beta_2 \Delta t}, \tag{68}$$

$$\alpha_3 = \frac{1}{\beta_2} - 1. \tag{69}$$

Considering Eqs. (67), (68), and (69), Eq. (66) can be written as

$$\ddot{\boldsymbol{u}}_{n+1} = \alpha_1(\boldsymbol{u}_{n+1} - \boldsymbol{u}_n) - \alpha_2\dot{\boldsymbol{u}}_n - \alpha_3\ddot{\boldsymbol{u}}_n. \tag{70}$$

Substituting Eq. (70) into Eq. (65), we obtain

$$\dot{\boldsymbol{u}}_{n+1} = \beta_1\alpha_2(\boldsymbol{u}_{n+1} - \boldsymbol{u}_n) + \left(1 - \frac{2\beta_1}{\beta_2}\right)\dot{\boldsymbol{u}}_n + \left(1 - \frac{\beta_1}{\beta_2}\right)\Delta t\ddot{\boldsymbol{u}}_n. \tag{71}$$

In the Newmark method the displacement solution $\boldsymbol{u}_{n+1}$ is obtained by Eq. (56). Then

$$\boldsymbol{M}\ddot{\boldsymbol{u}}_{n+1} + \boldsymbol{K}\boldsymbol{u}_{n+1} = \boldsymbol{f}_{n+1}. \tag{72}$$

Substituting Eqs. (70) and (71) into Eq. (72), we obtain

$$(\boldsymbol{K}_{n+1} + \alpha_1\boldsymbol{M}_{n+1})\boldsymbol{u}_{n+1} = \boldsymbol{f}_{n+1} + \boldsymbol{M}_{n+1}(\alpha_1\boldsymbol{u}_n + \alpha_2\dot{\boldsymbol{u}}_n + \alpha_3\ddot{\boldsymbol{u}}_n). \tag{73}$$

When $\boldsymbol{u}_{n+1}$ is calculated, $\dot{\boldsymbol{u}}_{n+1}$ and $\ddot{\boldsymbol{u}}_{n+1}$ are determined by Eqs. (70) and (71), respectively.

3.5 Numerical algorithm flow

Firstly, the initial calculation is performed as follows:

Step 1. From Eqs. (60) to (62), $\boldsymbol{M}$, $\boldsymbol{C}$, $\boldsymbol{K}$, and $\boldsymbol{f}$ are determined;

Step 2. Essential boundary condition is applied;

Step 3. $\boldsymbol{u}$, $\dot{\boldsymbol{u}}$, and $\ddot{\boldsymbol{u}}$ are set;

Step 4. Δt, β_1, and β_2 are set, and α_1, α_2, and α_3 are obtained.

Secondly, the time step is looped. For every time step,

Step 1. The payload is calculated at time $t + \Delta t$;

Step 2. According to Eq. (56), the displacement $\boldsymbol{u}_{t+\Delta t}$ at time $t + \Delta t$ is obtained;

Step 3. The velocity $\dot{\boldsymbol{u}}_{t+\Delta t}$ at time $t + \Delta t$ is found;

Step 4. The acceleration $\ddot{\boldsymbol{u}}_{t+\Delta t}$ at time $t + \Delta t$ is found;

Step 5. After the particle displacement vector $\boldsymbol{u}_{t+\Delta t}$ is obtained, the stress and strain of the particle are obtained according to Eqs. (2) and (3).

Finally, the time step cycle ends, and the particle displacement response, velocity, and stress are output. In this paper, the average acceleration method is adopted, which is an unconditionally stable integral scheme. Thus the new meshless method is formed.

4 Numerical examples

4.1 Vibration analysis of cantilever beam

As shown in Fig. 2, the cantilever beam subjected to a dynamic sudden load at the free end. The length and height of the cantilever beam are $l = 0.4$ m and $h = 0.05$ m, respectively. The material constants are Young's modulus $E = 200$ GPa, Poisson's ratio $\nu = 0.3$, and the density $\rho = 7850$ kg/m^3. The effect of damping is ignored. The sudden uniform tangential load $p(t) = 1000$ Pa is applied on the free end of the beam at time $t = 0$. As shown in

Figure 2 The cantilever beam subjected to a dynamic sudden load

Figure 3 The dynamic load

Figure 4 The node distribution of the cantilever beam
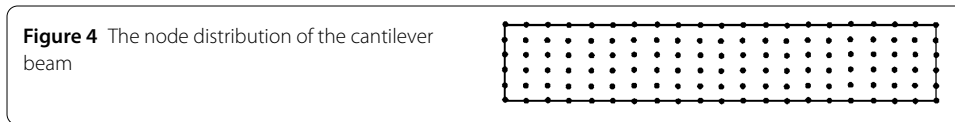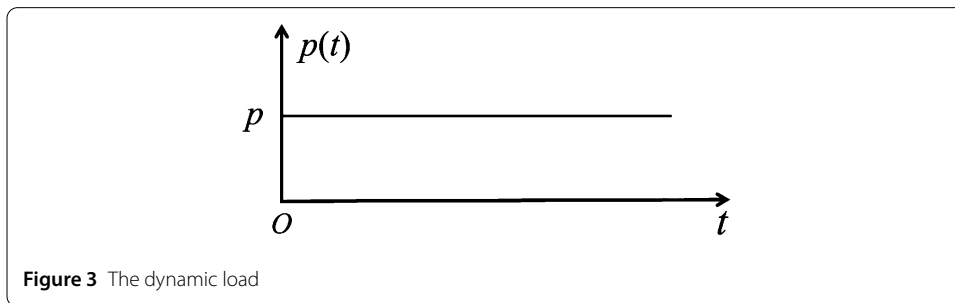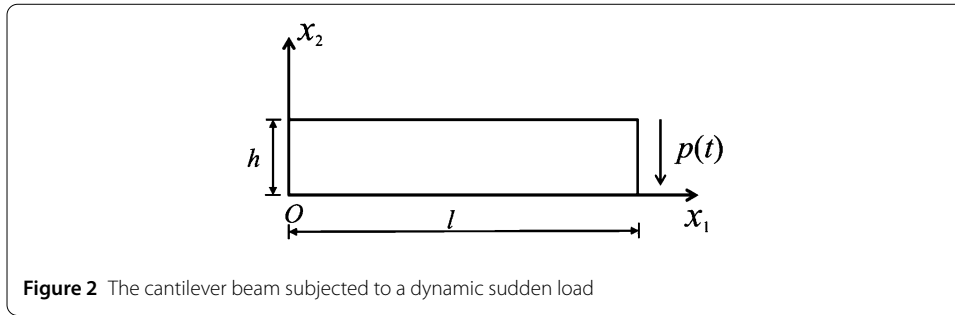
Fig. 3, ignoring the static load, the plane stress method is adopted to calculate. The displacement along the x_1 direction is u. The displacement along the x_2 direction is v. The initial conditions are $\boldsymbol{u}_0 = \dot{\boldsymbol{u}}_0 = 0$.

Analytic solution of deflection at the midpoint of the free end of the beam is

$$w(t) = \frac{1}{2}\left[1 - \cos\left(\frac{2\pi t}{T}\right)\right]w_{\max}, \tag{74}$$

where T and $w_{\max}$ are the natural vibration frequency of the cantilever beam and maximum deflection of the free end of the beam, respectively,

$$T = \frac{2\pi}{1.875^2}\sqrt{\frac{12\rho l^4}{Eh^2}}, \tag{75}$$

$$w_{\max} = \frac{2phl^3}{3EI}. \tag{76}$$

21×6 particles are used in the domain, as shown in Fig. 4. The cubic spline function is used as a weight function. The linear basis function is used as a base function. The time step chosen for the time integration is $\Delta t = 2 \times 10^{-6}$ s.

The solutions of the displacement at the free end midpoint of the beam obtained by IRKPM and analytical method are shown in Fig. 5. The comparison of the results calculated by IRKPM and analytical method is shown in Table 1, where R is the relative error, and the maximum relative error is 3.8%. Combining Fig. 5 and Table 1, we can see that IRKPM has a great precision and stability.

Figure 5 The time-dependent deflection of the midpoint of the free end
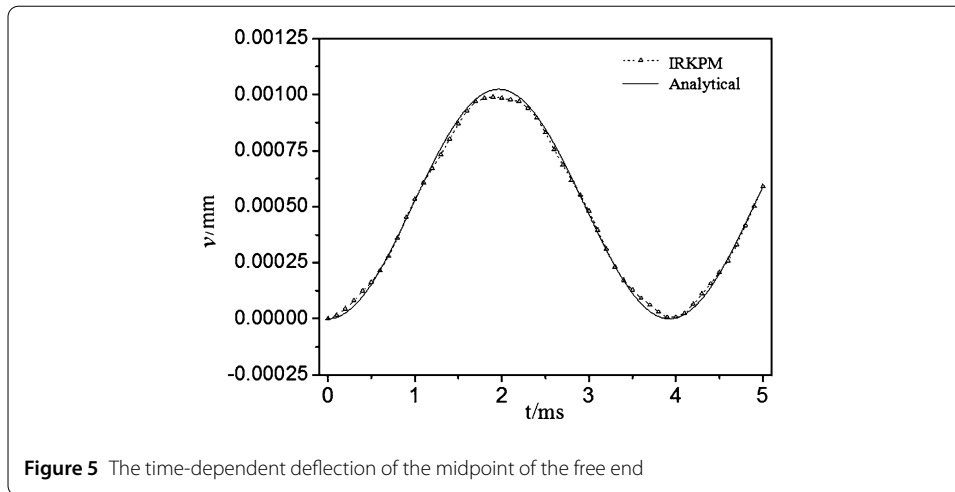
Table 1 The deflection of the midpoint of the free end

Time (ms)	IRKPM displacement v (10^{-4} mm)	Analysis displacement v (10^{-4} mm)	R
0	0	0	–
0.5	1.60	1.55	3.2%
1.0	5.32	5.27	0.9%
1.5	8.68	8.90	2.5%
2.0	9.84	10.23	3.8%
2.5	8.30	8.46	1.9%
3.0	4.79	4.66	2.8%
3.5	1.18	1.14	3.5%
4.0	0.04	0.04	0%
4.5	2.07	2.02	2.5%
5.0	5.90	5.89	0.2%

Figure 6 The cantilever beam under axial linear sudden load
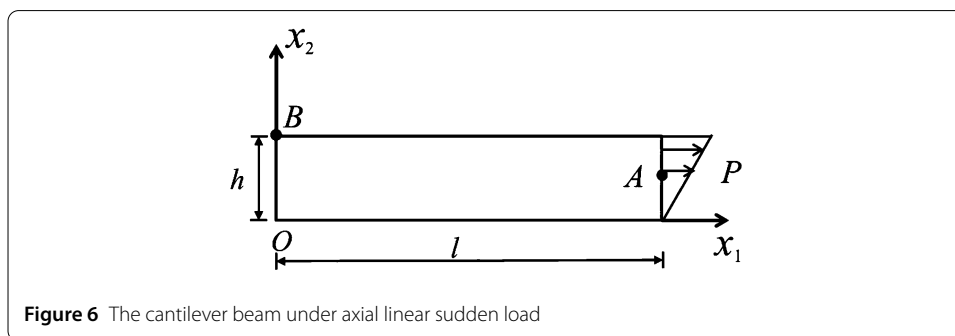
4.2 The dynamic response of cantilever beam under the axial sudden load

As shown in Fig. 6, the cantilever beam is under the sudden load in the axial direction. The geometric and physical parameters are as in Sect. 4.1. The effect of damping is ignored, and the sudden axial load $p(t) = 1$ GPa is applied on the free end of the beam at time $t = 0$. The sudden load remains the same.

21 $\times$ 6 particles are used in the domain. The cubic spline function is used as a weight function. The linear basis function is used as a base function. The mesh of the finite element method corresponds to the density of the particles.

Figure 7 The time-dependent displacement *u* at the point *A*

Figure 8 The time-dependent displacement *v* at the point *A*
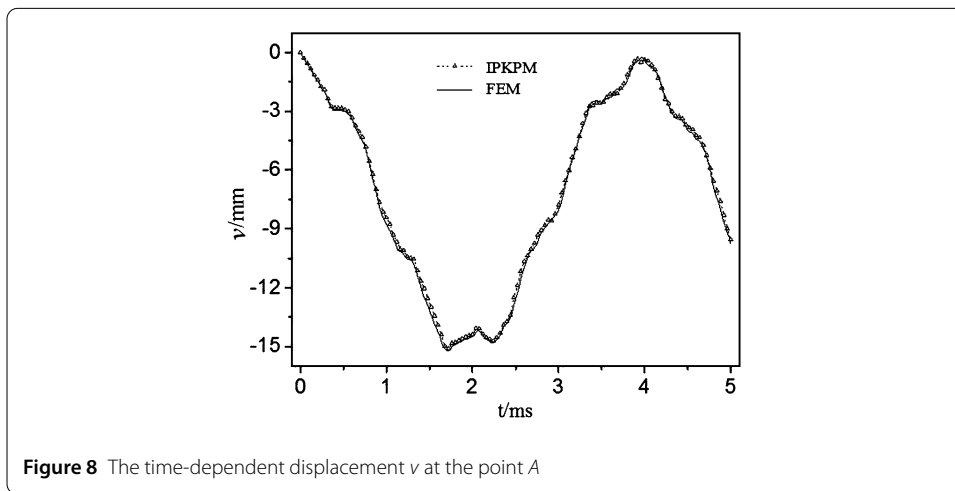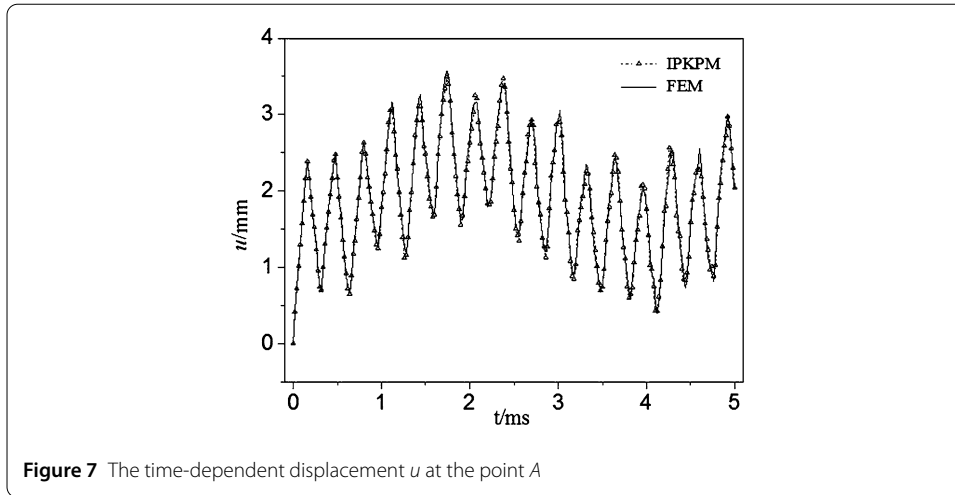
Table 2 The displacement *v* of the point *A*

Time (ms)	IRKPM displacement u (mm)	FEM displacement u (mm)	R	IRKPM displacement v (mm)	FEM displacement v (mm)	R
0	0	0	–	0	0	–
0.5	2.17	2.20	1.4%	−2.84	−2.88	1.4%
1.0	1.78	1.80	1.1%	−8.44	−8.50	0.7%
1.5	2.49	2.45	1.6%	−12.84	−12.90	0.5%
2.0	2.63	2.67	1.5%	−14.39	−14.43	0.3%
2.5	1.75	1.79	2.2%	−12.25	−12.30	0.4%
3.0	2.90	2.92	0.7%	−7.77	−7.81	0.5%
3.5	0.74	0.76	2.6%	−2.53	−2.56	1.2%
4.0	1.77	1.77	0%	−0.38	−0.39	2.6%
4.5	1.59	1.61	1.2%	−3.87	−3.90	0.8%
5.0	2.04	2.01	1.5%	−9.55	−9.59	0.4%

Figure 7 shows the time-dependent displacements *u* at the point *A* calculated by IRKPM and finite element method. Figure 8 shows the time-dependent displacements *v* at the point *A* calculated by IRKPM and finite element method.

Figure 9 The time-dependent stress σ_{11} at the point B
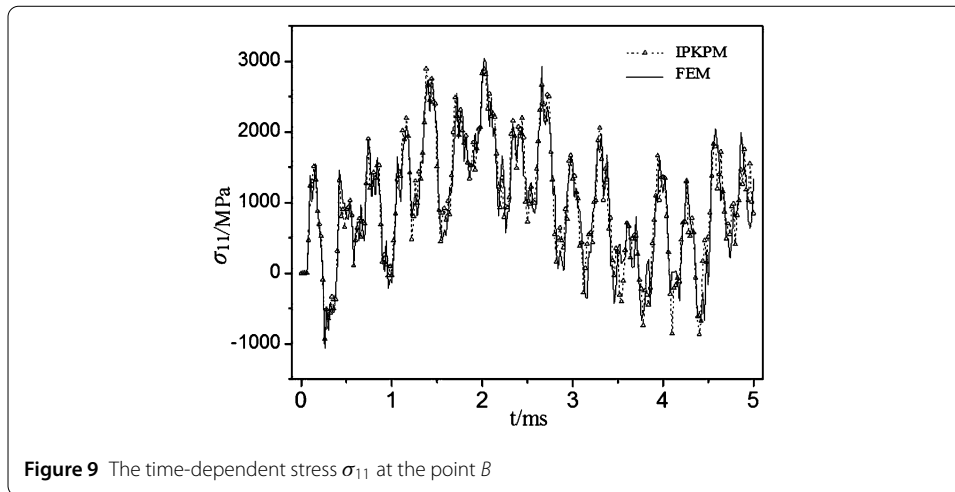
Table 2 shows the displacements of point A at different times calculated by the IRKPM and the finite element method, where R is the relative error. The maximum relative error of time-dependent displacement u is 2.6%. The maximum relative error of time-dependent displacement v is 2.6%. Figure 9 shows the time-dependent stress σ_{11} at point B.

5 Conclusions

The high-order smooth IRKPM for two-dimensional problems has been formed by combining the shape function of interpolated reproducing kernel particle method and the principle of virtual displacement of elastodynamics. The discrete form of the algorithm has been deduced subsequently.

This method has the advantage of applying the boundary conditions directly like the finite element method and improves the computational efficiency. The new method can be directly used in engineering more easily. Several examples show that the proposed method has higher accuracy and stability as dealing with two-dimensional elastokinetic problems.

Availability of data and materials
Not applicable.

Declarations

Competing interests
The authors declare no competing interests.

Author contributions
Jinpeng Gu and Yixiao Qin wrote the main manuscript text. Zhonghua Li prepared all figures. All authors reviewed the manuscript.

Author details
[1]College of Mechanical Engineering, Taiyuan University of Science and Technology, Taiyuan 030024, China. [2]Shantui Construction Machinery Co., Ltd, Jining 272000, China.

Publisher's Note

References

1. Ji, H.R., Li, D.X.: A novel nonlinear finite element method for structural dynamic modeling of spacecraft under large deformation. Thin-Walled Struct. **165**, 107926 (2021)
2. Leitner, M., Schanz, M.: Generalized convolution quadrature based boundary element method for uncoupled thermoelasticity. Mech. Syst. Signal Process. **150**, 107234 (2021)
3. Zhang, T., Li, X.L.: Meshless analysis of Darcy flow with a variational multiscale interpolating element-free Galerkin method. Eng. Anal. Bound. Elem. **100**, 237–245 (2017)
4. Peng, P.P., Cheng, Y.M.: Analyzing three-dimensional wave propagation with the hybrid reproducing kernel particle method based on the dimension splitting method. Eng. Comput. **38**, 1131–1147 (2022)
5. Liew, K.M., Zhao, X., Ferreira, A.: A review of meshless methods for laminated and functionally graded plates and shells. Compos. Struct. **93**, 2031–2041 (2011)
6. Liu, Z.S., Toh, W., Ng, T.Y.: Advances in mechanics of soft materials: a review of large deformation behavior of hydrogels. Int. J. Appl. Mech. **7**(5), 1530001 (2015)
7. Li, J., Sladek, J., Sladek, V., Wen, P.H.: Hybrid meshless displacement discontinuity method (MDDM) in fracture mechanics: static and dynamic. Eur. J. Mech. A, Solids **83**, 104023 (2020)
8. Granados, J.M., Bustamante, C.A., Florez, W.F.: Extending meshless method of approximate particular solutions (MAPS) to two-dimensional convection heat transfer problems. Appl. Math. Comput. **390**, 125484 (2021)
9. Hu, W., Trask, N., Hu, X.Z., Pan, W.X.: A spatially adaptive high-order meshless method for fluid-structure interactions. Comput. Methods Appl. Math. **355**, 67–93 (2019)
10. Qin, S.P., Wei, G.F., Tang, B.T.: The meshless analysis of elastic dynamic problem based on radial basis reproducing kernel particle method. Soil Dyn. Earthq. Eng. **139**, 106340 (2020)
11. Moghaddam, M.R., Baradaran, G.H.: Three-dimensional free vibrations analysis of functionally graded rectangular plates by the meshless local Petrov–Galerkin (MLPG) method. Appl. Math. Comput. **304**, 153–163 (2017)
12. Granados, J.M., Bustamante, C.A., Florez, W.F.: Extending meshless method of approximate particular solutions (MAPS) to two-dimensional convection heat transfer problems. Appl. Math. Comput. **390**, 125484 (2021)
13. Tang, Y.Z., Li, X.L.: Meshless analysis of an improved element-free Galerkin method for linear and nonlinear elliptic problems. Chin. Phys. B **26**(03), 219–229 (2017)
14. Lukyanov, A., Vuik, C.: A stable SPH discretization of the elliptic operator with heterogeneous coefficients. J. Comput. Appl. Math. **374**, 112745 (2020)
15. Abbaszadeh, M., Dehghan, M., Khodadadian, A., Heitzinger, C.: Analysis and application of the interpolating element free Galerkin (IEFG) method to simulate the prevention of groundwater contamination with application in fluid flow. J. Comput. Appl. Math. **368**, 112453 (2020)
16. Li, Q.H., Chen, S.S., Luo, X.M.: Using meshless local natural neighbour interpolation method to solve two-dimensional nonlinear problems. Int. J. Appl. Mech. **8**(5), 1650069 (2016)
17. Chen, S.S., Wang, J., Li, Q.H.: Two-dimensional fracture analysis of piezoelectric material based on the scaled boundary node method. Chin. Phys. B **25**(4), 040203 (2016)
18. Cheng, Y.M., Peng, M.J.: Boundary element-free method for elastodynamics. Sci. China Ser. G **48**(6), 641–657 (2005)
19. Cheng, Y.M., Wang, J.F., Li, R.X.: The complex variable element-free Galerkin (CVEFG) method for two-dimensional elastodynamics problems. Int. J. Appl. Mech. **4**(4), 1–23 (2012)
20. Elliott, A.J., Cammarano, A., Neild, S.A., Hill, T.L., Wagg, D.J.: Using frequency detuning to compare analytical approximations for forced responses. Nonlinear Dyn. **98**(2128), 2795–2809 (2019)
21. Chen, S.S., Wang, W., Zhao, X.S.: An interpolating element-free Galerkin scaled boundary method applied to structural dynamic analysis. Appl. Math. Model. **75**, 494–505 (2019)
22. Asareh, I., Yoon, Y.C., Song, J.H.: A numerical method for dynamic fracture using the extended finite element method with non-nodal enrichment parameters. Int. J. Impact Eng. **121**, 63–76 (2018)
23. Antil, H., Arndt, R., Rautenberg, C.N., Verma, D.: Nondiffusive variational problems with distributional and weak gradient constraints. Adv. Nonlinear Anal. **11**, 1466–1495 (2022)
24. Zha, S.X., Lan, H.Q.: Fracture behavior of pre-cracked polyethylene gas pipe under foundation settlement by extended finite element method. Int. J. Press. Vessels Piping **189**, 104270 (2021)
25. Milewski, S.: Higher order schemes introduced to the meshless FDM in elliptic problems. Eng. Anal. Bound. Elem. **131**, 100–117 (2021)
26. Rad, M.G., Shahabian, F., Hosseini, S.M.: A meshless local Petrov–Galerkin method for nonlinear dynamic analyses of hyper-elastic FG thick hollow cylinder with Rayleigh damping. Acta Mech. **226**(5), 1497–1513 (2015)
27. Gingold, R.A., Monaghan, J.J.: Smoothed particle hydrodynamics: theory and application to non-spherical stars. Mon. Not. R. Astron. Soc. **181**, 375–389 (1977)
28. Lucy, L.B.: A numerical approach to the testing of the fission hypothesis. Astron. J. **82**, 1013–1024 (1977)
29. Meng, J.N., Pan, G., Cao, Y.H.: Element-free Galerkin method for dynamic boundary flow problems. Mod. Phys. Lett. B **34**(24), 2050257 (2020)
30. Liu, Z., Wei, G.F., Wang, Z.M.: Numerical solution of functionally graded materials based on radial basis reproducing kernel particle method. Eng. Anal. Bound. Elem. **111**(C), 32–43 (2020)
31. Zhang, J.P., Wang, S.S., Gong, S.G., Zuo, Q.S., Hu, H.Y.: Thermo-mechanical coupling analysis of the orthotropic structures by using element-free Galerkin method. Eng. Anal. Bound. Elem. **101**, 198–213 (2019)
32. Watts, G., Pradyumna, S., Singha, M.K.: Free vibration analysis of non-rectangular plates in contact with bounded fluid using element free Galerkin method. Ocean Eng. **160**, 438–448 (2018)
33. Hu, D.A., Wang, Y.G., Li, Y.Y., Han, X., Gu, Y.T.: A meshfree-based local Galerkin method with condensation of degree of freedom elastic dynamic analysis. Acta Mech. Sin. **30**, 92–99 (2014)
34. Dehghan, M., Abbaszadeh, M.: Error analysis and numerical simulation of magnetohydrodynamics (MHD) equation based on the interpolating element free Galerkin (IEFG) method. Appl. Numer. Math. **137**, 252–273 (2019)

35. Dai, X.Q., Han, J.B., Lin, Q., Tian, X.T.: Anomalous pseudo-parabolic Kirchhoff-type dynamical model. Adv. Nonlinear Anal. **11**, 503–534 (2022)
36. Liu, W.K., Han, W.M., Lu, H.S., Li, S.F., Cao, J.: Reproducing kernel element method. Part I: theoretical formulation. Comput. Methods Appl. Math. **193**, 933–951 (2004)
37. Xiong, S.W., Martins, P.: Numerical solution of bulk metal forming processes by the reproducing kernel particle method. J. Mater. Process. Technol. **177**, 49–52 (2006)
38. Qin, Y.X., Liu, Y.Y., Li, Z.H., Yang, M.: An interpolating reproducing kernel particle method for two-dimensional scatter points. Chin. Phys. B **23**(7), 070207 (2014)
39. Qin, Y.X., Xie, W.T., Ren, H.P., Li, X.: Crane hook stress analysis upon boundary interpolated reproducing kernel particle method. Eng. Anal. Bound. Elem. **63**, 74–81 (2016)
40. Dai, B.D., Wang, Q.F., Zhang, W.W., Wang, L.H.: The complex variable meshless local Petrov–Galerkin method for elastodynamic problems. Appl. Math. Comput. **243**, 311–321 (2014)
41. Shojaei, A., Mossaiby, F., Zaccariotto, M., Galvanetto, U.: The meshless finite point method for transient elastodynamic problems. Acta Mech. **228**, 3581–3593 (2017)
42. Mirzaei, D., Hasanpour, K.: Direct meshless local Petrov–Galerkin method for elastodynamic analysis. Acta Mech. **227**(3), 619–632 (2016)
43. Wen, P.H., Aliabadi, M.H.: Elastodynamic problems by meshless local integral method: analytical formulation. Eng. Anal. Bound. Elem. **37**(5), 805–811 (2013)
44. Huang, X.J., Wen, P.H.: Meshless local integral equation method for two-dimensional nonlocal elastodynamic problems. J. Phys. Conf. Ser. **734**(3), 032131 (2016)
45. Dai, B.D., Wei, D.D., Zhang, Z., Ren, H.P.: The complex variable meshless local Petrov–Galerkin method for elastodynamic analysis of functionally graded materials. Appl. Math. Comput. **309**, 17–26 (2017)
46. Teng, F., Lou, Z.D., Yang, J.: A natural boundary element method for the Sobolev equation in the 2D unbounded domain. Bound. Value Probl. **2017**, 179 (2017)